Journal of Japan Association for Earthquake Engineering, Vol. 21, No. 3, 2021

# INVESTIGATION OF STORY STIFFNESS IDENTIFICATION OF TORSIONALLY COUPLED SHEAR BUILDINGS USING MODAL PARAMETERS

Masanori HORIKE[1] and Eiko NISHIHARA[2]

[1] Member, Advisor, Division of Engineering, Hanshin Consultants Co., Ltd,
Osaka, Japan, horike@hanshin-consul.co.jp
[2] Group Leader, Architectural Group, NEWJEC Inc.,
Osaka, Japan, nishiharako@newjec.co.jp

**ABSTRACT**: A method is proposed to identify the story stiffness matrix of torsionally coupled shear buildings story by story, using the modal parameters extracted from Green's functions. Numerical tests reveal that although the method is valid, robustness to noise is low. In particular, the stiffnesses of the top story are greatly underestimated due to non-cancellation of noise, indicating that noise-reduced modal parameters are of importance for identification. An application of the method to an existing building reveals that knowledge of the precise masses and moments of inertia of individual floors is required in advance, and that velocity recordings and their decomposition into three degrees of freedom using a precise location of the center of gravity may reduce noise of the modal parameters.

**Keywords**: Identification, Story stiffness matrix, Modal parameter, Torsionally coupled shear buildings, Robustness to noise

## 1. INTRODUCTION

The assessment of vulnerability of buildings to a damaging earthquake is a key issue for ensuring their safety. For this purpose, it is desirable to non-destructively detect deteriorated or damaged portions and assess their extent and degree. An approach of detecting changes in stiffness using vibration recordings is one that meets this requirement. The changes are obtained by comparing the stiffnesses identified from vibration recordings at the beginning and end of a certain period (for example, before and after a damaging earthquake). Hence, the non-destructive detection of the stiffness change eventually reduces to the development of a high-precision identification method for the stiffness property using recordings of earthquake responses, microtremors, and forced vibrations.

There have been many studies on development of identification methods for building stiffness, broadly classified into four approaches. The first approach is based on the optimization problem which minimizes the objective function that represents the squared difference between observables and corresponding predictables. As the observables, earthquake responses[1)], frequency responses[2), 3)], and modal parameters[4)–6)], specifically the natural frequency, the damping ratio, and the eigenvector (or shape function), have been used.

The second approach is based on the state-space model of building vibrations. Luş et al.[7)] developed

a method for identifying the mass, stiffness, and damping ratio using an identified state-space model. They also confirmed the robustness of the method to noise through numerical tests[8]. Kim and Lynch[9] applied it to an experimental building to reliably detect change in the stiffness property.

The third employs vibration equations of individual floors which are derived from the vibration equation of a whole building. These individual equations contain only the stiffness and damping ratio of the story immediately below individual floors, whereby they are identified story by story without being affected by those of the other stories. This approach, however, needs the mass and moment of inertia prior to the identification of the stiffness. Nakamura and Yasui[10] applied this method to existing shear buildings before and after the 1995 Hyogoken Nanbu Earthquake, and detected the reduction of stiffnesses using microtremor vibration recordings. Omrani et al.[11] extended this approach to torsionally coupled shear buildings (TCSBs). Assuming that floors vibrate only horizontally, they derived the vibration equations of the individual floors with respect to three degrees of freedom (3DOF) from global vibration equation explicitly shown by Ueng et al.[12] and verified it with synthetic vibration data of a benchmark structure. Subsequently, they[13] applied it to experimental data of microtremor vibration and free vibration recorded in test structures with intentionally created damages. It revealed that this method successfully detects even minor change in stiffness property and is robust to mass uncertainties. Nakamiya et al.[14] attempted to improve the accuracy of identified stiffnesses, replacing the coefficient matrix and the constant vector estimated from experimental data in the story-wise vibration equation with those estimated from GFs.

The final approach is to employ neural networks. González and Zapico[15] developed a damage identification method based on a conventional neural network, in which the modal parameters are used as input data and the mass and stiffness are obtained as output data. Detection methods based on deep learning using a convolutional neural network have also been proposed. There are studies on crack detection where this approach is applied to image processing[16] and on damage detection of simple beams using waveform recordings as input data[17].

Recent studies proposed methods that use the vibration equations differently from the aforementioned third class. Shintani et al.[18] derived simultaneous linear equations to determine all stiffnesses and damping coefficients of a whole building simultaneously. However, this way of determination may propagate identification errors to the physical parameters of all stories[11]. Nabeshima and Takewaki[19] proposed a different method to estimate the stiffness of the story of interest in TCSBs using the frequency-domain equilibrium equation above that story. In addition, they conducted numerical tests and vibration experiments with a shaking table to examine the accuracy and the robustness to noise. This method, however, is still impractical due to two requirements imposed on TCSBs: the coincidence of horizontal locations of the centers of the gravity of all floors and the uniaxial eccentricity.

As described above, many story stiffness identification methods have been developed. However, most of them deal only with a single degree of freedom for translational motion, despite most low- and middle- rise buildings being eccentric buildings that have an offset between the locations of the center of gravity and the center of stiffness. A coupling occurs between the translational and rotational motions in the vibrations of these buildings. Hence, it is necessary for damage detection and aseismic diagnosis of the eccentric buildings to develop a method for identifying the story stiffness matrix with a more realistic vibration model. To our knowledge, Omrani et. al.[11], cited previously, firstly developed a practical tool in identifying the story stiffness matrix of TCSBs. However, this method has a drawback that the stiffness matrix varies with input motions, as described in detail in section 2.

Thus, the first aim of this study is development of an identification method that can be applied to TCSBs without this drawback. It is achieved by introduction of the secular equation of the eigenvalue problem for vibrations of TCSBs. This equation determines the story stiffness and damping matrices only with the modal parameters. Hence, the next issue is estimation of accurate modal parameters from vibration recordings.

Not much work has been done on the identification of story stiffness with the modal parameters. Charaverty[20] developed an identification method using the two elements of the eigenvector at the 1st and top floors and the natural frequencies, utilizing the assumption that the mass and stiffness distribution are assigned as their ratios to respective reference values. The advantage of this method is

that experiments of vibration measurement are relatively easy, and the disadvantage is that it requires knowledge of the distribution of the mass and stiffness, which severely limits applicability in terms of buildings covered. Michael et al.[21] developed an identification method that assumes only the mass of a unit area. The natural frequency and eigenvector are first estimated from microtremor recordings by the FDD method[22], and then the story stiffnesses are determined, putting the natural frequency and eigenvector into the formula derived from the vibration equation of each floor. Instead of using the modal parameters for the identification of the story stiffness, Ikeda[23] proposed to use them for creation of constraints to ensure that the modal parameters observed are consistent with those computed. Adding these constraints to the vibration equations of individual floors, reliable story stiffness is determined. As mentioned previously, these methods also deal only with a single degree of freedom for translational motion and coupled vibrations are out of the scope.

In order for our new identification method to be a practical and reliable tool, it requires easy vibration measurement and accurate estimation of modal parameters. The first requirement is satisfied with microtremor measurements and the second requirement is satisfied with the modal parameters extracted from Green's functions (GFs) that are inferred from microtremor recordings by the Wiener filter[24]. GFs inferred by the Wiener filter have an advantageous property of noise reduction[25] so the modal parameters extracted from them are also expected to be less noisy. Despite such a property, these modal parameters have not been used for the identification of story stiffness. The modal parameters of an existing TCSB have been already obtained in Horike and Hada[26, 27] with the procedure mentioned above. A subsequent goal therefore is to apply the proposed identification method to the existing TCSB where precise modal parameters are already available. Thus, the second aim of this study is to examine practicability of the newly proposed identification method through numerical tests and the application to the existing TCSB, using less noisy modal parameters extracted from GFs obtained from microtremor recording by the Wiener filter.

In section 2, we introduce the identification method in detail. In section 3, we perform numerical tests to investigate the validity of the method and the robustness to noise. In section 4, we briefly recapitulate descriptions of the existing TCSB and the modal parameters obtained in Horike and Hada[26, 27], particularly their reliability. In section 5, we apply the identification method to the building. The application to existing buildings is important for discovering issues affecting practical use that cannot be obtained from numerical tests and experiments using model buildings. Comparing identified story matrices with those used for the structural design, we discuss the causes of the discrepancies between them and clarify the issues involved in the identification process. Also, we examine an improvement of the method by adjusting the masses and moments of inertia. In section 6, we make several proposals for noise reduction of GFs based on the survey of noise sources. Finally, we summarize the findings in this study.

We make substantial reference to the preceding two papers (Horike and Hada[26, 27]). For convenience, they are hereinafter referred to as the 1st and 2nd papers.

## 2. METHOD FOR IDENTIFICATION OF STORY STIFFNESS MATRIX

This section provides a detailed description of an identification method. A global stiffness matrix of an n-story TCSB is composed of n matrices with a size of 3 × 3[11, 12]. Assuming that a global damping matrix is also specified in the same manner as the global stiffness matrix, the equation of vibration for a whole building is decomposed into the equations of vibration of individual floors[11], which include only the story stiffness and damping matrices immediately below their floors. They are written as

$$[[K]_\ell[C]_\ell]\{D(t)\}_\ell = -\sum_{j=\ell}^{n}[M]_j\{\ddot{X}(t)\}_j, \quad (\text{t}=1,2,\cdots,\ n_t) \quad \text{for } (\ell = 1,2,\cdots,n), \tag{1}$$

where $[K]_\ell$ and $[C]_\ell$ denote the story stiffness and damping matrices of the $\ell$-th story. Matrix $[M]_j$ is the mass matrix of the $j$-th floor which is specified as

$$[M]_j = \begin{bmatrix} m & 0 & 0 \\ 0 & m & 0 \\ 0 & 0 & I \end{bmatrix}_j, \qquad (j = 1,2,\cdots,n). \tag{2}$$

Letters $m$ and $I$ respectively denote the mass and the moment of inertia. Notation $\{\ddot{X}(t)\}_j$ designates the acceleration vector of the 3DOF which is composed of two translational motions and torsional motion. Letters $t$ and $n_t$ are integers of discrete time and their number.

The 3DOF acceleration vector of the $j$-th floor $\{\ddot{X}(t)\}_j$ is the sum of the 3DOF relative acceleration vector of the $j$-th floor $\{\ddot{u}_1(t)\ \ddot{u}_2(t)\ \ddot{u}_3(t)\}_j^T$ and the 3DOF acceleration vector of the basement $\{\ {}_0\ddot{y}_1(t)\ \ {}_0\ddot{y}_2(t)\ \ {}_0\ddot{y}_3(t)\}^T$, referred to simply as the input vector. Superscript $T$ denotes transpose. The 3DOF relative acceleration vector is computed by the numerical integration of the convolution shown in the following equation

$$\ddot{u}_i(t) = \sum_{j=1}^{3}\sum_{\tau=0}^{n_g} g_{ij}(\tau)\ {}_0\ddot{y}_j(t-\tau) \qquad (i = 1,2,3), \tag{3}$$

where $g_{ij}$ is GF and subscripts $i$ and $j$ denote the directions of the input and output motions, respectively.

The coefficient vector $\{D(t)\}_\ell$ is written as

$$\{D(t)\}_\ell = \begin{Bmatrix} \{U(t)\}_\ell - \{U(t)\}_{\ell-1} \\ \{\dot{U}(t)\}_\ell - \{\dot{U}(t)\}_{\ell-1} \end{Bmatrix}, \tag{4}$$

where the velocity vector $\{\dot{U}(t)\}_\ell = \{\dot{u}_1(t), \dot{u}_2(t), \dot{u}_3(t)\}_\ell^T$ and the displacement vector $\{U(t)\}_\ell = \{u_1(t), u_2(t), u_3(t)\}_\ell^T$ are respectively obtained by numerical integration of the 3DOF relative acceleration vector once and twice.

It is obvious from the above descriptions that given the input vector and GFs, Eq. (1) determines the story stiffness and damping matrices story by story without propagating identification errors from one story to another, which is an advantage of this equation. It, however, has a drawback. Despite the story stiffness and damping matrices being constant by nature, those determined by this equation vary with the input vector due to dependence of the constant vector $\{D(t)\}$ on the input vector through the velocity vector $\{\dot{U}(t)\}$ and the displacement vector $\{U(t)\}$. To retain the advantages of Eq. (1) and to erase the drawback, we develop an alternative method: the secular equations of the eigenvalue problem for individual floors. We derive these equations from Eq. (1) as follows.

Setting the input vector $\{\ {}_0\ddot{y}_1(t)\ \ {}_0\ddot{y}_2(t)\ \ {}_0\ddot{y}_3(t)\}^T$ to zero vector, Eq. (1) reduces to a homogeneous differential equation. Assuming that a solution of this differential equation of the $\ell$-th floor is $\{U(t)\}_\ell = \{\ {}_sV\}_\ell e^{\lambda t}$ and putting it into the equation, we obtain the secular equation specified as

$$\left[[K][C]\right]_\ell \{\ {}_sE\}_\ell = -\ {}_s\lambda^2 \sum_{j=\ell}^{n}[M]_j \{\ {}_sV\}_j \qquad (s = 1,2,\cdots,n_m) \quad \text{for } (\ell = 1,2,\cdots,n). \tag{5}$$

Here, ${}_s\lambda$ and $\{\ {}_sV\}_j$ denote the eigenvalue and eigenvector of the $s$-th mode. Notation $n_m$ denotes a modal number. Vector $\{\ {}_sE\}_\ell$ consists of the eigenvalue and eigenvector, and is specified as

$$\{\ {}_sE\}_\ell = \begin{Bmatrix} \{\ {}_sV\}_\ell - \{\ {}_sV\}_{\ell-1} \\ {}_s\lambda\{\ {}_sV\}_\ell - \ {}_s\lambda\{\ {}_sV\}_{\ell-1} \end{Bmatrix}. \tag{6}$$

We can see that given the eigenvalue and eigenvector, Eqs. (5) and (6) enable us to identify the stiffness

and damping story matrices story by story. Also, it is obvious that the input vector does not influence the identification at all.

It is noted that the secular equation is homogeneous and linear with respect to the eigenvector so that it is not determined uniquely, and an arbitrary constant factor times eigenvector also meets this equation. More precisely, this multiplicative factor is required only to be invariant from floor to floor.

The participation vector (hereafter PV) is related to the eigenvector by the equation specified as

$$\left\{ {}_sp_{1j} \;\; {}_sp_{2j} \;\; {}_sp_{3j} \right\}_\ell^T = {}_s\beta_j \left\{ {}_sV \right\}_\ell \qquad (\ell = 1,2,\cdots,n), \tag{7}$$

where notation ${}_s\beta_j$ denotes the participation factor which depends on the input motion and the modal order designated respectively by subscripts *j* and *s*, but on neither the floor number designated by subscript $\ell$ nor the output motion (first of the two rear subscripts). Thereby, the PVs also meet Eq. (5). We use the eigenvector for the numerical test of the identification method in section 3 and use the PV for the practical application in section 5.

The right-hand side of Eq. (7) shows that for each mode there are three PVs depending on the three input motions designated by subscript *j* and that they share the same eigenvector. This means that we can select a single noise-reduced PV from among the three for each mode. This is an advantage of using the PVs.

## 3. NUMERICAL TEST

The stiffness matrix of the $\ell$-th story is written as

$$[K]_\ell = \begin{bmatrix} \sum k_{x_i} & 0 & -\sum k_{x_i} y_i \\ 0 & \sum k_{y_i} & \sum k_{y_i} x_i \\ -\sum k_{x_i} y_i & \sum k_{y_i} x_i & \sum k_{x_i} y_i^2 + \sum k_{y_i} x_i^2 \end{bmatrix}_\ell = \begin{bmatrix} k_{11} & 0 & -k_{13} \\ 0 & k_{22} & k_{23} \\ -k_{31} & k_{32} & k_{33} \end{bmatrix}_\ell \tag{8}$$

where $k_{x_i}$ and $k_{y_i}$ are the stiffnesses of lateral load resisting elements such as columns and braces along the two horizontal axes, and $x_i$ and $y_i$ are their locations. Replacing the elements specified by the polynomials in the middle matrix with parameters of $k_{ij}$, the stiffness matrix is simply rewritten as the rightmost matrix. Our targets for identification are not the stiffnesses of individual resisting elements ($k_{x_i}$ and $k_{y_i}$) but the reduced ones ($k_{ij}$). Looking at the stiffness matrix, we immediately notice two properties: symmetricity and positive values of the three diagonal elements $k_{11}$, $k_{22}$, and $k_{33}$. These two properties also hold true for the damping matrix. We will use these two properties for the evaluation of the two identified story matrices.

Numerical tests are conducted to investigate the validity and robustness to noise. A building for the tests is an 11-story TCSB and the structural parameters such as the mass, moment of inertia, and the elements of the story matrix are given in Table 1. The story damping matrix is a stiffness proportional matrix with a proportional constant of 0.02.

Prior to the numerical tests, eigenvalue and eigenvector preparation is required. They are yielded by solving the general eigenvalue problem with the structural parameters in Table 1. The natural frequencies and damping ratios derived from the eigenvalues are listed up to the 6th mode in Table 2. Also, the absolute values for the three elements of the eigenvectors are shown in Fig. 1.

Putting these eigenvalues and eigenvectors into Eqs. (5) and (6), we identify the two matrices, which reveal that all the stiffnesses shown in Table 1 are reproduced with high precision of up to four or more digits, and the damping ratios are also reproduced with the same precision. Furthermore, even if the low-order three modes are used, we can get the same degree of precision in reproduction of the two matrices. These results of the numerical tests show that the proposed identification method is valid.

Table 1 Structural parameters of the building for the numerical tests

| Floor or story | Mass (x10^5 kg) | Moment of inertia (x10^5 kg m$^2$) | $k_{11}$ (x10^8 N/m) | $k_{22}$ (x10^8 N/m) | $k_{13}$ (x10^7 N) | $k_{23}$ (x10^8 N) | $k_{33}$ (x10^11 N m) |
|---|---|---|---|---|---|---|---|
| 1 | 9.50 | 4.34 | 9.41 | 7.47 | 22.57 | -28.70 | 3.79 |
| 2 | 9.07 | 4.13 | 10.85 | 8.42 | 14.08 | -19.41 | 4.30 |
| 3 | 9.01 | 4.09 | 9.43 | 7.65 | 9.27 | -17.86 | 4.03 |
| 4 | 9.00 | 4.09 | 9.05 | 7.27 | 2.42 | -17.09 | 3.87 |
| 5 | 8.97 | 4.07 | 8.82 | 7.09 | 6.63 | -16.61 | 3.78 |
| 6 | 8.44 | 3.83 | 8.50 | 6.93 | 6.53 | -14.76 | 3.58 |
| 7 | 8.47 | 3.85 | 7.57 | 6.30 | 10.62 | -7.26 | 3.32 |
| 8 | 8.35 | 3.79 | 7.34 | 5.89 | -3.83 | -2.18 | 3.07 |
| 9 | 8.33 | 3.78 | 7.16 | 5.54 | -7.08 | -1.53 | 2.92 |
| 10 | 10.20 | 4.62 | 6.77 | 5.11 | -1.72 | -1.78 | 2.71 |
| 11 | 3.25 | 1.44 | 5.66 | 4.37 | -2.16 | -1.93 | 2.31 |

Table 2 Natural frequencies and damping ratios of the building for the numerical tests

| Mode order | Natural frequency (Hz) | Damping ratio |
|---|---|---|
| 1 | 0.638 | 0.0401 |
| 2 | 0.722 | 0.0453 |
| 3 | 0.735 | 0.0562 |
| 4 | 1.8 | 0.113 |
| 5 | 1.98 | 0.125 |
| 6 | 2.05 | 0.129 |

The robustness of the method to noise is examined. For this purpose, we yield eigenvectors contaminated with noise. At first, we generate two independent random numbers corresponding to the real and imaginary parts of the noise on an assumption of uniform distribution between $\pm 1$, using different seed numbers for the two parts. Then, noise level is adjusted by giving the ratio of the square root of the sum of squares of the two random numbers to the absolute value of the eigenvector element. The noise generated in this way is added to all three elements of the eigenvectors, which yields the eigenvectors contaminated with noise.

The numerical tests are performed for the three noise levels: 1%, 3%, 5%. They reveal that the two identified story matrices are not symmetric for every story even in the case of the lowest noise level of 1%. This means that the inference of noise-reduced GFs is a crucial issue for identification, because the eigenvalues and eigenvectors are extracted from GFs. Meanwhile, the diagonal elements of the two matrices, namely $k_{11}$, $k_{22}$, $k_{33}$, $c_{11}$, $c_{22}$, and $c_{33}$, take positive values even in the case of the highest noise level of 5%, indicating that they may be reliable and comparatively robust to noise. For the accuracy check of the diagonal elements of the two matrices, we then compare those in the three cases of the noise levels to true values of the corresponding diagonal elements in Table 1. Results of these comparisons are shown in Fig. 2 as the ratios of the identified values to the true values.

The upper three diagrams exhibit the ratios of the stiffness, while the lower three exhibit the ratios of the damping ratio. We immediately notice that noise influences the identification appreciably. In particular, the damping ratio is more sensitive to noise than the stiffness, probably due to its small value. Also, we find a conspicuous feature common to the three stiffnesses, $k_{11}$, $k_{22}$, and $k_{33}$ in that the stiffness at the top story is greatly underestimated. Although this feature is not so conspicuous in the

damping ratios, it is visible in them as well. Non-cancellation of noise at the top floor accounts for the extreme underestimation.

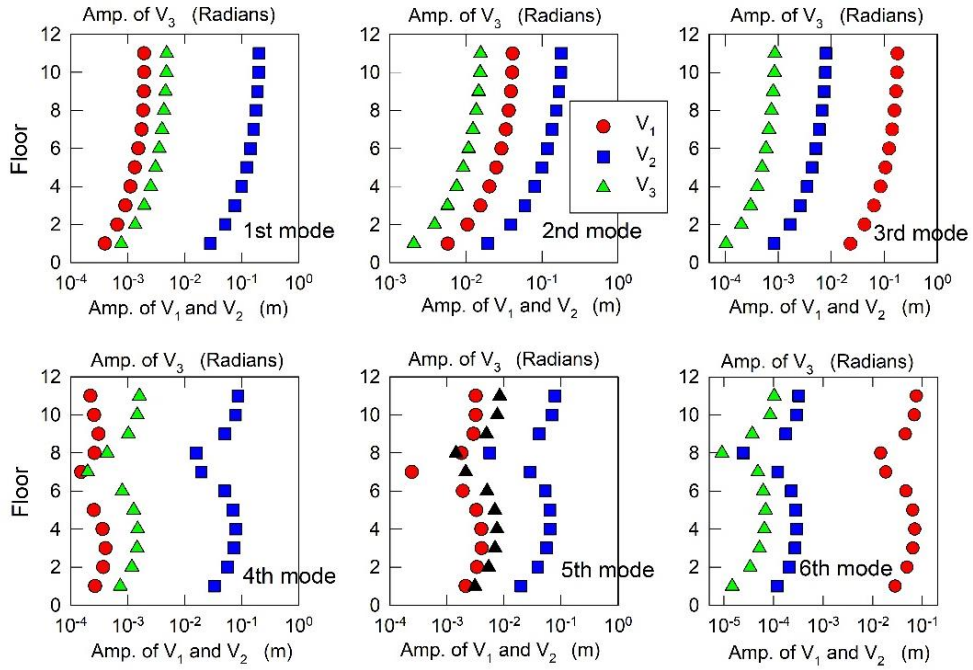


Fig. 1 Absolute values of the three elements of the eigenvectors of the building for numerical tests up to the 6th mode. The lower horizontal axis is for elements $V_1$ and $V_2$ and the upper is for $V_3$

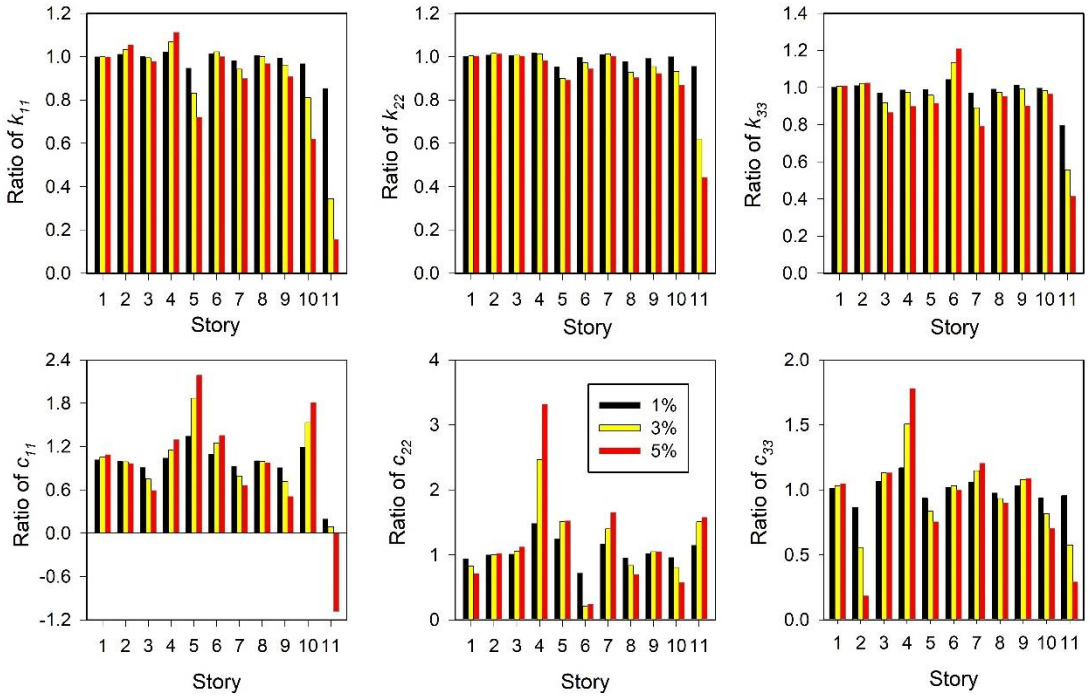


Fig. 2 Ratios of identified three diagonal elements to counterparts listed in Table 1 for stiffness matrices (top three diagrams) and for damping matrices (bottom three diagrams)

As can be seen in the right-hand side of Eq. (5), the eigenvectors contaminated with noise are stacked over the floors from the floor of interest (i.e., the $\ell$-th floor) to the top floor. However, this stacking is impossible at the top floor, with the result that the stiffnesses and the damping ratios produce underestimates at this floor.

The numerical tests reveal that the identification method proposed is valid but is significantly sensitive to noise. This indicates that inference of noise-reduced GFs is a key issue for identifying story stiffness matrices.

## 4. BUILDING AND MODAL PARAMETERS

In this section we describe the building subject to identification of the story stiffness matrices and the modal parameters used for the identification. These are already described in detail in the 1st and 2nd papers, so here we only recapitulate them briefly.

This 8-story building is used for offices, and is a frame structure composed of steel reinforced concrete columns and steel girders. The structural parameters are listed in Table 3, which shows that this building is definitely a torsionally coupled shear building because of the existence of off-diagonal elements of the story stiffness matrix (i.e., $k_{13}$ and $k_{23}$).

Table 3 Structural parameters of the existing TCSB

| Floor or story | Mass (x10^5 kg) | Moment of inertia (x10^7 kg m$^2$) | $k_{11}$ (x10^9 N/m) | $k_{22}$ (x10^9 N/m) | $k_{13}$ (x10^9 N) | $k_{23}$ (x10^8 N) | $k_{33}$ (x10^11 N m) |
|---|---|---|---|---|---|---|---|
| 1 | 8.84 | 12.55 | 8.05 | 4.39 | 20.84 | -140.20 | 7.83 |
| 2 | 7.87 | 8.45 | 9.15 | 4.07 | 25.12 | 4.41 | 6.03 |
| 3 | 7.80 | 8.48 | 8.03 | 3.07 | 20.10 | 17.46 | 4.34 |
| 4 | 7.68 | 8.33 | 6.81 | 2.63 | 14.62 | 12.46 | 4.78 |
| 5 | 7.48 | 8.53 | 6.40 | 2.29 | 12.65 | 7.85 | 4.46 |
| 6 | 7.59 | 8.65 | 6.01 | 1.98 | 10.58 | 5.78 | 4.20 |
| 7 | 7.51 | 8.71 | 5.45 | 1.62 | 7.48 | 3.34 | 3.80 |
| 8 | 11.24 | 9.78 | 4.67 | 1.20 | 2.24 | 0.82 | 3.85 |

Experiments of microtremor measurement were implemented during the period between 0:00 am to 5:00 am to avoid the effects of human activities inside the building as well as nearby traffic outside the building as much as possible. We additionally measured wind velocities during microtremor experiments to investigate their effects on building vibrations, whereby we found that there were no effects of the wind on GFs (1st paper). The extraction of the modal parameters from these GFs was performed using the genetic algorithm and was fully described in the 2nd paper.

The GFs were inferred from microtremor recordings which were band-pass-filtered in the frequency range between 1 Hz and 10 Hz. Use of a band-pass filter with an adequate frequency range is important because it enables the GFs to contain only less-noise modes. The low- and high-frequency limits were determined with different criteria. Fourier spectra of torsional motion of the basement decrease rapidly below a certain frequency that is mainly controlled by the length of the basement and S wave velocity of sediments. Meanwhile, the Fourier spectra of the GFs related to torsional motion conversely increase rapidly below this frequency due to the decrease in the spectra of torsional motion of the basement[28]. Hence, the low-frequency limit was determined at the frequency where the spectra of the GFs related to torsional motion begin to increase.

The high-frequency limit was determined in a different way. There are conspicuous peak frequencies which appear commonly in the Fourier spectra of multiple GFs. The high-frequency limit was determined as the frequency where spectra are sufficiently small and higher than the highest peak frequency. We searched for appropriate frequency limits by trial and error with the criteria mentioned

above. We finally found that the low-frequency limit of 1 Hz and the high-frequency limit of 10 Hz were appropriate. The band-pass filter with this frequency range produced the GFs having the five conspicuous peak frequencies as shown in Fig. 14 of the 1st paper.

The accuracy of the GFs inferred from microtremor recordings in the frequency range between 1 Hz and 10 Hz was scrutinized for their waveforms in Fig.12 of the 1st paper and for their Fourier spectra. As a result, the GFs inferred from microtremor recordings are considered to be appreciably accurate.

## 5. APPLICATION TO AN EXISTING TCSB

We apply the identification method to the existing TCSB using the observed modal parameters. The extraction of the modal parameters of this building from the GFs is fully described in the 2nd paper. The eigenvalues consist of the natural frequencies and damping ratios, the observed values for which are listed in Table 4, which is the same as Table 5 in the 2nd paper. As mentioned in section 2, we use the PVs instead of the eigenvectors in this section because we have already extracted not the eigenvectors, but the PVs. The absolute values of the PVs are also exhibited in Fig. 3. We selected the PVs with less noise from the observed PVs exhibited in Fig. 12 of the 2nd paper.

Table 4 Observed natural frequencies and damping ratios

| Mode order | Natural frequency (Hz) | Damping ratio |
|---|---|---|
| 1 | 1.64 | 0.019 |
| 2 | 1.95 | 0.026 |
| 3 | 3.07 | 0.035 |
| 4 | 6.37 | 0.018 |

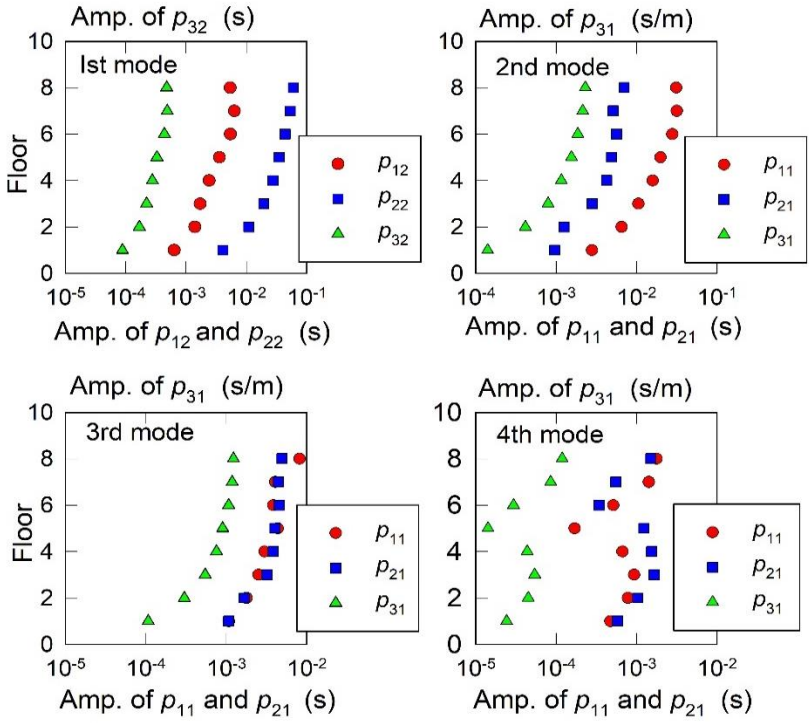


Fig. 3 Absolute values of the three elements of the PVs of the existing building up to the 4th mode

Putting these eigenvalues and the PVs into Eqs. (5) and (6), we identify the two matrices for all the stories. Unfortunately, neither of the matrices are symmetric, and hence the off-diagonal elements ($k_{12}$, $k_{13}$, $c_{12}$, $c_{13}$) of all the stories are unreliable, judging from the common property of the two matrices, i.e. symmetricity, as described in section 3. Meanwhile, the diagonal elements of the stiffness matrix and those of the damping matrices produce different results: those of the damping matrices ($c_{11}$, $c_{22}$, and $c_{33}$) of all the stories are mixed with positive and negative values, but those of the stiffness matrices ($k_{11}$, $k_{22}$, and $k_{33}$) take positive values alone. This suggests that only the diagonal elements of the stiffness matrices are reliable. Hence, our concern is confined to only the diagonal elements in the following evaluation.

We then evaluate their accuracy (Fig. 4). They are shown as the ratios of the identified stiffnesses to the counterparts in Table 3 with the black bars. The identified stiffnesses of $k_{11}$ and $k_{22}$ are obviously underestimated for almost all stories, while the element of $k_{33}$ is overestimated except for the top story. The causes for these discrepancies cannot be other than errors in the structural parameters in Table 3 and noise included in the eigenvalues in Table 4 and in the PVs extracted from the GFs in Fig. 3. The effects of the noise are definitely visible in the two diagonal elements of $k_{11}$ and $k_{33}$ at the top story which are greatly underestimated. These underestimations are primarily due to non-cancellation of the noise included in the PVs, as indicated by the numerical tests.

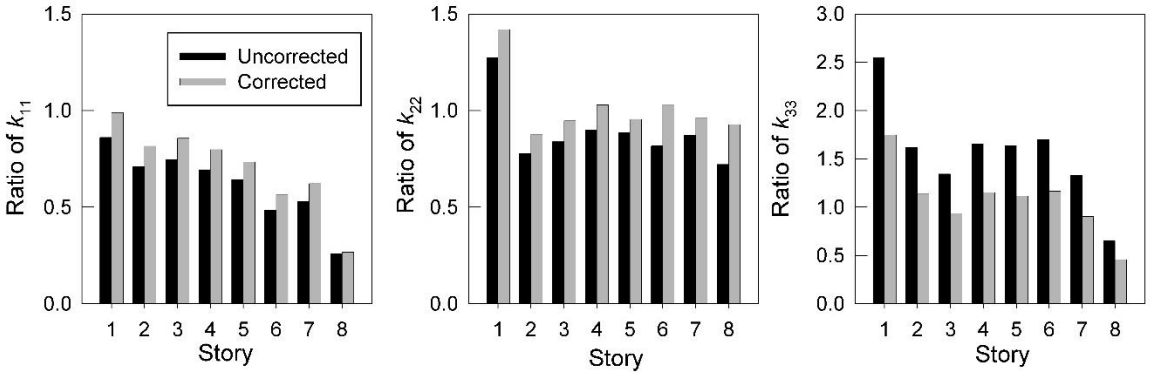


Fig. 4 Ratios of identified diagonal elements of the stiffness matrix to the stiffnesses used for the structural design. Black and gray bars are respectively ratios of stiffnesses identified using uncorrected and corrected masses and moments of inertia

We examine the effects of the errors of the structural parameters on the identification. This is important for applying the identification method to existing buildings, because it is implemented on an assumption that the masses and moments of inertia are true values. Comparing the natural frequencies extracted from the GFs up to the 5th mode, exhibited in the second column of Table 5, with those computed using the structural parameters in Table 3, exhibited in the 5th column, they are quite different. For example, the observed natural frequency of the 1st mode is 1.64 Hz against 1.71 Hz for the computed frequency. This suggests that the mass and moment of inertia should be adjusted prior to the identification of the stiffness in use of Eq. (5). Although the natural frequency is in general influenced by the mass and moment of inertia as well as by the stiffnesses, we assume in this paper that only the mass and moment of inertia are variable when fitting the observed natural frequencies to the computed ones; the stiffnesses are fixed for convenience. Although the observed natural frequencies and damping ratios are shown in Table 4 up to the 4th mode, only the natural frequency of the 5th mode is judged to be sufficiently reliable and is added to Tables 5 and 6.

We conduct a two-step identification. First, optimum values of the masses and the moments of inertia, which minimize the difference between the computed and observed natural frequencies, are determined. Then, putting these optimum values into Eq. (5), the stiffnesses are identified. For simplicity of the first step, we determine the two magnification factors alone: one is for the masses and the other is for the moments of inertia.

The natural frequencies observed and computed at the first step are shown in Table 5 for the comparison. The natural frequencies observed for the first five modes are exhibited in the 2nd column, while those exhibited in the 3rd to 5th columns are obtained with numerical computation for conditions that the magnification factor for the moments of inertia changes between 0.8 times and 1.0 times, but the masses are fixed to the structural design values. The natural frequencies of the 1st and 5th modes in these three columns do not vary at all, despite the change of the moments of inertia. This means that these two modes are primarily related to the translational motion which is weakly coupled with the torsional motion, and the natural frequencies of the two modes are almost unaffected by the moment of inertia. In other words, the masses can be determined, fitting the natural frequencies observed to those computed for the two modes alone.

The observed natural frequencies of these two modes are lower than the calculated ones, indicating the need for increment of the masses. This building is used for offices, and the total mass of desks, shelves, documents, books, etc. required for office work is quite large. Hence, an increase in the masses is appropriate.

We determine the optimum masses. Varying only the magnification factor of the masses between 1.0 times and 1.2 times, we obtain the natural frequencies exhibited in the 5th to 9th columns. We select the optimal masses which minimize the sum of absolute values of the non-dimensional residual between the observed and calculated natural frequency. It is referred to as the residual sum and is defined as $\sum_s |{}_sf_{obs} - {}_sf_{cal}| / {}_sf_{obs}$, where ${}_sf_{obs}$ and ${}_sf_{cal}$ respectively denote the observed and calculated natural frequencies of the $s$-th mode. The residual sum of the natural frequencies of the 1st and 5th modes is shown at the bottom of Table 5. It turns out that it is better to increase the masses from 1.1 times to 1.15 times.

Table 5 Natural frequencies to determine optimal masses

| Mode order | Observed NF (Hz) | Computed NF (Hz) | | | | | | |
|---|---|---|---|---|---|---|---|---|
| | | 0.8I 1.0m | 0.9I 1.0m | 1.0I 1.0m | 1.0I 1.05m | 1.0I 1.1m | 1.0I 1.15m | 1.0I 1.2m |
| 1 | 1.64 | 1.71 | 1.71 | 1.71 | 1.67 | 1.63 | 1.60 | 1.57 |
| 2 | 1.96 | 2.21 | 2.12 | 2.04 | 2.02 | 2.01 | 2.00 | 1.99 |
| 3 | 3.07 | 2.97 | 2.92 | 2.89 | 2.83 | 2.78 | 2.73 | 2.68 |
| 4 | 6.37 | 6.45 | 6.2 | 5.96 | 5.92 | 5.89 | 5.85 | 5.80 |
| 5 | 6.75 | 7.23 | 7.23 | 7.23 | 7.05 | 6.89 | 6.74 | 6.60 |
| Residual sum of 1st and 5th modes | | 0.114 | 0.114 | 0.114 | 0.0627 | 0.0268 | 0.0259 | 0.065 |

NF: abbreviation of natural frequency

We next determine optimal moments of inertia. The natural frequencies computed for the structural parameters in Table 3 are exhibited in the 5th column. The natural frequency of the 2nd mode is higher than the observed frequency exhibited in the 2nd column, while the natural frequencies of the 3rd and 4th modes are lower than those observed, indicating that adjustment of the moments of inertia alone cannot account for the observed natural frequencies. We therefore adjust both the moments of inertia and masses, and pick up their optimum values which minimize the residual sum of the natural frequencies for all five modes.

The natural frequencies are computed for conditions of 1.1 times the masses and a magnification factor of the moments of inertia ranging from 0.7 times to 0.9 times. The resulting frequencies are exhibited in the 3rd to 5th columns in Table 6. Meanwhile, the natural frequencies, computed for conditions of 1.15 times the masses and a magnification factor of the moments of inertia ranging from 0.6 times to 0.9 times, are exhibited in the 6th to 9th columns. The residual sums in this table show that

1.15 times the masses and 0.7 times the moments of inertia are optimum.

We identify the stiffness matrices with the optimum values of 1.15 times the masses and 0.7 times the moments of inertia. The stiffnesses identified reliably are again the diagonal elements of the stiffness matrices for the same reasons as the identification implemented with the structural design values of masses and moments of inertia. Thus, our concern is again confined to the three diagonal elements of the stiffness matrices.

All three diagonal elements identified are shown in Fig. 4 as gray bars indicating their ratio to the stiffnesses used for the structural design. The agreement with the stiffnesses of the structural design is improved significantly. In particular, stiffnesses $k_{22}$ show a better agreement with those used for structural design except for the 1st story. This improvement indicates the need to prepare accurate masses and moments of inertia in advance of the stiffness identification.

However, there are still discrepancies in stiffnesses $k_{11}$ and $k_{33}$: stiffnesses $k_{11}$ are still underestimated, especially at the top three stories, and stiffnesses $k_{33}$ are still overestimated except for the top story. Also, stiffnesses $k_{11}$ and $k_{33}$ are greatly underestimated at the top floor, again indicating that inference of noise-reduced GFs is a key issue.

Table 6 Natural frequencies to determine optimum masses and moments of inertia

| Mode order | Observed NF (Hz) | Computed NF (Hz) | | | | | | |
|---|---|---|---|---|---|---|---|---|
| | | 0.7I 1.1m | 0.8I 1.1m | 0.9I 1.1m | 0.6I 1.15m | 0.7I 1.15m | 0.8I 1.15m | 0.9I 1.15m |
| 1 | 1.64 | 1.63 | 1.63 | 1.63 | 1.60 | 1.64 | 1.64 | 1.60 |
| 2 | 1.96 | 2.25 | 2.17 | 2.10 | 2.28 | 2.22 | 2.15 | 2.07 |
| 3 | 3.07 | 2.98 | 2.89 | 2.82 | 3.1 | 2.95 | 2.85 | 2.79 |
| 4 | 6.37 | 6.50 | 6.32 | 6.11 | 6.55 | 6.42 | 6.25 | 6.06 |
| 5 | 6.75 | 6.90 | 6.90 | 6.90 | 6.76 | 6.76 | 6.75 | 6.75 |
| Residual sum | | 0.226 | 0.202 | 0.222 | 0.227 | 0.181 | 0.187 | 0.220 |

## 6. DISCUSSION AND CONCLUSION

We investigated the effects of errors of the structural parameters, especially the mass and moment of inertia, and their adjustment resulted in a partial improvement. The search for optimum masses and moments of inertia in a more sophisticated way may improve the agreement between the identified stiffnesses and the stiffnesses used for the structural design. However, it is not expected that the agreement between the two will be achieved only by adjusting the structural parameters, because we can definitely recognize the effect of noise contained in PVs on the identification, especially through extreme underestimates of stiffnesses $k_{11}$ and $k_{33}$ at the top story and of stiffness $k_{11}$ at the 6th and 7th stories.

Looking carefully at Fig. 3, we can understand what the noise is. All three elements of the PVs of the first three modes are expected to monotonically increase their absolute values toward the upper floor, as is seen in Fig. 1. However, this is not always the case at the 6th and higher floors. For example, looking at $p_{12}$, an element of PV of the 1st mode, the amplitude at the top floor is decreasing rather than increasing. Also, the amplitudes of $p_{11}$ and $p_{21}$, elements of the PV of the 3rd mode, change irregularly at the 6th floor and above it. We therefore consider that the GFs were not properly estimated for these floors. Since the PVs were inferred from the GFs, we consider that the errors included in the PVs were propagated from errors in the GFs. If this is the case then, a further question arises: where does the noise in the GFs come from? One possible source is an error in the location of the center of gravity.

GFs are inferred not from microtremor recordings, but from the 3DOF into which microtremor recordings are decomposed. The center of gravity is required for this decomposition. Hence, if there is an error in the position of the center of gravity, noise contaminates the GFs, and propagates to the modal parameters. Thereby, an error in the position of the center of gravity can be considered as a cause of the underestimation of the stiffness of the 6th or the stories above it. In addition, the position of the center of gravity is necessary for the determination of the moment of inertia. Accurate determination of the center of gravity is accordingly important for accurate estimation of GFs and for the identification as well.

Another possible source of noise is the physical quantity (displacement, velocity or acceleration) for the microtremor recordings. Since the accuracy of observation equipment has been rapidly improving recently, it may not be necessary to consider noise generation due to numerical integration. However, acquisition of the appropriate physical quantity contributes to noise reduction.

It is preferable to acquire microtremor recordings not with acceleration but with velocity for two reasons. The first reason is that since the formula decomposing vibration recordings into 3DOF is rigorous only for velocity recordings, no error is generated by the decomposition of velocity recordings into 3DOF. The second reason is related to the inference of GFs associated with rotations. In the 1st paper, it was demonstrated that low-frequency noise appears in these GFs inferred from acceleration 3DOF, unless the low-frequency contents are removed. However, if we infer GFs associated with rotations from velocity 3DOF, low-frequency noise in the GFs is very small, so that the noise in the GFs estimated from the velocity 3DOF is smaller than the noise in the GFs estimated from the acceleration 3DOF. To summarize the above discussion on observations, it is better to acquire velocity recordings and estimate GFs from them using accurate centers of gravity.

Ignoring the effects of rocking motions of the basement also increases the noise in the PVs. We assume in this study that all floors including the basement vibrate only horizontally. However, this assumption may not be realistic; the noise seems to be larger in the PVs at the higher floors, as is seen in Fig 3. Hence, the GFs associated with the translational motions may be contaminated with noise due to non-correction of the effects of the rocking motions of the basement. The PVs extracted from these GFs may be also contaminated with noise accordingly.

So far, we have discussed the improvements in the modal parameter estimation procedure used in the 1st and 2nd papers. There are, however, different methods to estimate the modal parameters from stationary vibration recordings such as microtremors. In particular, the random decrement method, abbreviated as RD method, may be preferable in that it does not require the input motions, as opposed to our method using the Wiener filter that requires the input motions. Ueng et al.[12] extended the RD method to be applicable to TCSBs. Consequently, modal parameters estimated by this extended RD method may improve the accuracy of identified story stiffnesses.

We have developed an identification method for the story stiffness matrices of torsionally coupled shear buildings using the modal parameters. This method has advantages: the story stiffness matrices are identified story by story without propagating identification errors from one story to another as well as without the effects of input motions. To make use of these advantages, the precise masses and moments of inertia of individual floors and the noise-reduced modal parameters are required in advance of application of the method. The noise-reduced modal parameters are extracted from GFs that are obtained from velocity microtremor recordings using the precise location of the center of gravity. Furthermore, the effects of the rocking motions of the basement may be required in considering the inference of the GFs related to translational motions. These improvements lead to identification in which not only diagonal elements, but also off-diagonal elements, are obtained accurately.

## ACKNOWLEDGEMENTS

The authors benefited greatly from discussions with Prof. Yoshiki Ikeda at the Disaster Prevention Research Institute of Kyoto University. The paper was significantly improved by reviews from the three anonymous reviewers and the referee.

## REFERENCES


1) Kang, J. S., Park, S. K., Shin, S. and Lee, H. S.: Structural System Identification in Time Domain Using Measured Acceleration, *Journal of Sound and Vibration*, Vol. 288, Nos. 1–2, pp. 215–234, 2005.
2) Garcia-Palencia, A. J. and Santini-Bell, E.: A Two-Step Model Updating Algorithm for Parameter Identification of Linear Elastic Damped Structures, *Computer-aided Civil and Infrastructure Engineering*, Vol. 28, No. 7, pp. 509–521, 2013. https://doi.org/10.1111/mice.12012
3) Li, J., Law, S. S. and Ding, Y.: Substructure Damage Identification based on Response Reconstruction in Frequency Domain and Model Updating, *Engineering Structures*, Vol. 41, pp. 270–284, 2012,
4) Ren, W.-X. and Chen, H.-B.: Finite Element Model Updating in Structural Dynamics by Using the Response Surface Method, *Engineering Structures*, Vol. 32, No. 8, pp. 2455–2465, 2010. https://doi.org/10.1016/j.engstruct.2010.04.019
5) Jaishi, B. and Ren, W.-X.: Structural Finite Element Model Updating Using Ambient Vibration Test Results, *Journal of Structural Engineering*, Vol. 131, No. 4, pp. 617–628, 2005.
6) Skolnik, D., Lei, Y., Yu, E. and Wallace, J. W.: Identification, Model Updating, and Response Prediction of an Instrumented 15-Story Steel-Frame Building, *Earthquake Spectra*, Vol. 22, No. 3, pp. 781–802, 2006. https://journals.sagepub.com/doi/abs/10.1193/1.2219487
7) Luş, H., De Angelis, M., Betti, R. and Longman, R. W.: Constructing Second-Order Models of Mechanical Systems from Identified State Space Realizations. Part I: Theoretical Discussions, *Journal of Engineering Mechanics*, Vol. 129, No. 5, pp. 477–488, 2003. https://doi.org/10.1061/(ASCE)0733-9399(2003)129:5(477)
8) Luş, H., De Angelis, M., Betti, R. and Longman, R.W.: Constructing Second-Order Models of Mechanical Systems from Identified State Space Realizations. Part II: Numerical Investigations, *Journal of Engineering Mechanics*, Vol. 129, No. 5, pp. 489–501, 2003. https://doi.org/10.1061/(ASCE)0733-9399(2003)129:5(489)
9) Kim, J. and Lynch, J. P.: Subspace System Identification of Support Excited Structures-Part II: Gray-Box Interpretations and Damage Detection, *Earthquake Engineering and Structural Dynamics*, Vol. 41, No. 22, pp. 2253–2271, 2012. https://doi.org/10.1002/eqe.2185
10) Nakamura, M. and Yasui, Y.: Damage Evaluation of a Steel Structure Subjected to Strong Earthquake Motion Based on Ambient Vibration Measurements, *Journal of Structural and Construction Engineering (Transactions of AIJ)*, Vol. 64, No. 517, pp. 61–68, 1999. https://doi.org/10.3130/aijs.64.61_1
11) Omrani, R., Hudson, R. E. and Taciroglu, E.: Story-by-Story Estimation of the Stiffness Parameters of Laterally-Torsionally Coupled Buildings Using Forced or Ambient Vibration Data: I. Formulation and Verification. *Earthquake Engineering and Structural Dynamics*, Vol. 41, pp. 1609–1634, 2012. https://doi.org/10.1002/eqe.1192
12) Ueng, J.-M., Lin, C.-C. and Lin, P.-L.: System Identification of Torsionally Coupled Buildings, *Computers and Structures*, Vol. 74, No. 6, pp. 667–786, 2000. https://doi.org/10.1016/S0045-7949(99)00073-5
13) Omrani, R., Hudson, R. E. and Taciroglu, E.: Story-by-Story Estimation of the Stiffness Parameters of Laterally-Torsionally Coupled Buildings Using Forced or Ambient Vibration Data: II. Application to Experimental Data. *Earthquake Engineering and Structural Dynamics*, Vol. 41, No. 12, pp. 1635–1649, 2012. https://doi.org/10.1002/eqe.1193
14) Nakamiya R., Horike, M., Hada, K. and Nishimura, T.: Estimation of Stiffness and Damping Layer Matrices for Torsionally Coupled Structure: Part 1, Identification Method and Numerical Tests, *Proceedings of the Annual Convention of Architectural Institute of Japan,* Vol. 2 pp. 637–638, 2013.
15) González, M. P. and Zapico, J. L.: Seismic Damage Identification in Building Using Neural Networks and Modal Data, *Computers and Structures*, Vol. 86, pp. 416–426, 2008.
16) Cha, Y.-J., Choi, W. and Büyüköztürk, O.: Deep Learning-Based Crack Damage Detection Using Convolutional Neural Networks, *Computer-Aided Civil and Infrastructure Engineering*, Vol. 32, No. 5, pp. 361–378, 2017.

17) Lin, Y.-Z., Nie, Z.-H. and Ma, H.-W.: Structural Damage Detection with Automatic Feature-Extraction through Deep Learning, *Computer-Aided Civil and Infrastructure Engineering*, Vol. 32, No. 5, pp. 1025–1046, 2017. https://doi.org/10.1111/mice.12313
18) Shintani, S., Yoshitomi, S. and Takewaki, I.: Direct Linear System Identification Method for Multistory Three-Dimensional Building Structure with General Eccentricity, *Frontiers in Built Environment*, Vol. 3, 2017. https://doi.org/10.3389/fbuil.2017.00017
19) Nabeshima, K. and Takewaki, I.: Frequency-Domain Physical-Parameter System Identification of Building Structures with Stiffness Eccentricity, *Frontiers in Built Environment*, Vol. 3, 2017. https://doi.org/10.3389/fbuil.2017.00071
20) Chakraverty, C.: Identification of Structural Parameters of Multistorey Shear Buildings from Modal Data, *Earthquake Engineering and Structural Dynamics*, Vol. 34, No. 6 pp. 543–554, 2005. https://doi.org/10.1002/ege.431
21) Michel, C., Guéngen, P. and Bard, P.-Y.: Dynamic Parameters of Structure Extracted from Ambient Vibration Measurements: An Aid for the Seismic Vulnerability Assessment of Existing Buildings in Moderate Seismic Hazard Regions, *Soil Dynamics and Earthquake Engineering*, Vol. 28, No. 8, pp. 593–604, 2008.
22) Brincker, R. Zhang, L. and Anderson, P.: Modal Identification of Output-Only System Using Frequency Domain Decomposition, *Smart Materials and Structures*, Vol. 10, No. 3, pp. 441–445, 2001. https://doi.org/10.1088/0964-1726/10/3/303
23) Ikeda, Y.: Identification of Story Stiffness for MDOF Shear Building Structures Considering Consistency with Modal Information, *Journal of Structural and Construction Engineering (Transactions of AIJ)*, Vol. 74, No. 646, pp. 2237–2243, 2009.
24) Robinson, E. A.: *Multichannel Time Series Analysis with Digital Computer Programs,* 2nd ed., Goose Pond Press, Houston, Texas, 454 pp., 1983.
25) Chen, J., Benesty, J., Huang, Y. and Doclo, S.: New Insights into the Noise Reduction Wiener Filter, *IEEE Transactions on Audio, Speech, and Language Processing,* Vol. 14, No. 4, pp. 1218–1234, 2006.
26) Horike, M. and Hada, K.: Green's Functions Estimated from Microtremor Recordings for a Torsionally Coupled Shear Building by the Wiener Filter Technique, *Journal of Japan Association for Earthquake Engineering*, Vol. 18, No. 2, pp. 184–202, 2018.
27) Horike, M. and Hada, K.: A Two-Step Determination of Modal Parameters for Torsionally Coupled Shear Buildings Using Green's Functions, *Journal of Japan Association for Earthquake Engineering*, Vol. 19, No. 2, pp. 87–106, 2019. https://doi.org/10.5610/jaee.19.2_87
28) Yasugi, N. Hada, K. and Horike, M.: Effects of Wind and Data Length on Green's Functions of Torsionally Coupled Buildings and Correction of Green's Functions Associated with Rotation, *Journal of Japan Association for Earthquake Engineering*, Vol. 16, No. 1 (Special Issue), pp. 139–150, 2016.

**(Submitted: April 1, 2020)**
**(Accepted: January 5,2021)**